

Plasma vertical position control with internal coils in CFETR

Mei-Xia Chen(陈美霞), Bin Wu(吴斌), Yong Guo(郭勇), Cheng-Yue Liu(刘成岳)
Citation: Chin. Phys. B. 35, 095203 (2026). DOI: 10.1088/1674-1056/ae6565 |
CSTR: 32038.14.CPB.ae6565
http://cpb.iphy.ac.cn; http://iopscience.iop.org/cpb

What follows is a list of articles you may be interested in

Calculation and prediction of divertor detachment via impurity seeding by using one-dimensional model

Wen-Jie Zhou(周文杰), Xiao-Ju Liu(刘晓菊), Xiao-He Wu(邬潇河), Bang Li(李邦), Qi-Qi Shi(石奇奇), Hao-Chen Fan(樊皓尘), Yan-Jie Yang(杨艳杰), Guo-Qiang Li(李国强)
Chin. Phys. B. 33, 085205 (2024). DOI: 10.1088/1674-1056/ad426a

Magnetic diagnostics layout design for CFETR plasma equilibrium reconstruction

Qingze Yu(于庆泽), Yao Huang(黄耀), Zhengping Luo(罗正平), Yuehang Wang(汪悦航), Zijie Liu(刘自结), Wangyi Rui(芮望颐), Kai Wu(吴凯), Bingjia Xiao(肖炳甲), Jiangang Li(李建刚)
Chin. Phys. B. 33, 045201 (2024). DOI: 10.1088/1674-1056/ad23d6

Numerical study of alpha particle loss with toroidal field ripple based on CFETR steady-state scenario

Niuqi Li(李钮琦), Yingfeng Xu(徐颖峰), Fangchuan Zhong(钟方川), Debing Zhang(张德兵)
Chin. Phys. B. 33, 015202 (2024). DOI: 10.1088/1674-1056/ad03de

Discrete Alfvén eigenmodes in the CFETR steady-state scenario

Yuan-Dan Lan(兰源丹), Shuang-Hui Hu(胡双辉), Si-Jie Ouyang(欧阳思杰), Wan-Po Zhu(朱万坡), Xuan-Ge Huang(黄旋格)
Chin. Phys. B. 32, 055201 (2023). DOI: 10.1088/1674-1056/aca397

Parametric decay instabilities of lower hybrid waves on CFETR

Taotao Zhou(周涛涛), Nong Xiang(项农), Chunyun Gan(甘春芸), Guozhang Jia(贾国章), Jiale Chen(陈佳乐)
Chin. Phys. B. 31, 095201 (2022). DOI: 10.1088/1674-1056/ac67c2

Plasma vertical position control with internal coils in CFETR

Mei-Xia Chen(陈美霞)[1], Bin Wu(吴斌)[2], Yong Guo(郭勇)[2,†], and Cheng-Yue Liu(刘成岳)[1,‡]

[1] *School of Physics, Hefei University of Technology, Hefei* 230009, *China*
[2] *Institute of Plasma Physics, Chinese Academy of Science, Hefei* 230026, *China*

(Received 3 January 2026; revised manuscript received 26 April 2026; accepted manuscript online 28 April 2026)

Plasma vertical displacement events (VDEs) are critically important in tokamak operation and design due to their direct influence on plasma performance and device safety. For the China Fusion Engineering Test Reactor (CFETR) — China's next-generation tokamak currently in its conceptual design phase — particular emphasis must therefore be placed on developing reliable VDE control strategies. The Tokamak Simulation Code (TSC) and TokSys have been widely applied in VDE studies on multiple tokamaks worldwide, including DIII-D, EAST, JT-60U, and ITER. A key parameter for characterizing vertical instability is the plasma vertical growth rate. In this work, free-drift plasma evolution was simulated using TSC, and the vertical growth rate was extracted by fitting the plasma vertical position trajectory — a result consistent with predictions from TokSys. Furthermore, active feedback control of VDEs in CFETR has been implemented in TSC for three representative internal control (IC) coil configurations: mounted on the inner vacuum vessel wall, on the outer wall of the blanket, and on the inner wall of the blanket. The corresponding IC coil current control waveforms obtained from TSC have also been benchmarked against TokSys simulations.

Keywords: CFETR, vertical displacement active control, TSC, TokSys

PACS: 52.50.–b, 52.55.Fa, 52.65.–y

DOI: 10.1088/1674-1056/ae6565 **CSTR:** 32038.14.CPB.ae6565

1. Introduction

From an economic perspective, achieving a beta value of approximately 10% is crucial for the viability of commercial tokamak-based fusion reactors. Consequently, enhancing the beta value has become a critical research priority within the global fusion community. A widely adopted approach to increasing this value in existing devices involves elongating the plasma cross-section to achieve a divertor configuration. A high elongation ratio offers significant benefits for plasma performance, a topic that has been thoroughly investigated in both theoretical and experimental studies.[1] However, such elongated plasmas are susceptible to vertical displacement events (VDEs) — a type of vertical instability that, if not actively controlled, can cause the plasma to come into contact with the vessel wall, leading to discharge disruption. During such disruption events, severe and potentially damaging effects may occur, including high thermal loads, substantial mechanical stress, and the generation of runaway electrons.[2] Therefore, it is necessary to implement a robust feedback control system to actively stabilize the plasma against vertical motion.

The China Fusion Engineering Test Reactor (CFETR)[3] is a next-generation tokamak facility in China, designed to bridge the gap between ITER and DEMO. With a targeted fusion power ($P_{\rm fus}$) of 1 GW, a high duty factor ranging from 0.3 to 0.5, and tritium self-sufficiency achieved through a tritium breeding ratio (TBR) > 1, CFETR represents a critical step toward the practical application of fusion energy. The standard lower single null (LSN) configuration of CFETR, illustrated in Fig. 1, enables flexible plasma shaping with an elongation of 2, a major radius of 7.2 m, a minor radius of 2.2 m, and a plasma current of 14 MA. The main parameters of CFETR are listed in Table 1, while the geometric parameters of the coils are provided in Table 2. Compared with the EAST device, CFETR incorporates a blanket structure, making it more representative of future fusion reactors. VDE control in the presence of the blanket structure presents significant challenges and novel research opportunities. The simulation results are of forward-looking significance for ITER operation and fusion reactor design.

The Tokamak Simulation Code (TSC)[4–6] and TokSys[7] have been extensively applied to VDE studies on various tokamaks worldwide, including JT-60U,[8] DIII-D,[9] ITER,[10] and EAST.[11] Specifically, for DIII-D, the TSC plasma halo model, structural models, and initial conditions for the time evolution of VDEs are discussed. For ITER, research focuses on vertical stability analysis, structural design, vertical position feedback control analysis, and the impact of initial conditions on vertical motion. For EAST, a passive plate system and an IC system are modeled to control vertical instability, while the IC PS capability is discussed based on the maximum controllable vertical displacement.

The TSC is a numerical model of an axisymmetric

†Corresponding author. E-mail: yguo@ipp.ac.cn
‡Corresponding author. E-mail: cyliu@hfut.edu.cn

© 2026 Chinese Physical Society and IOP Publishing Ltd. All rights, including for text and data mining, AI training, and similar technologies, are reserved.

tokamak that simulates the evolution of a two-dimensional time-dependent free-boundary plasma by advancing the MHD equations coupled with the external circuits. It also solves the 1D flux-surface-averaged transport equations for energy, particles, and current density utilizing predefined transport coefficients. The TokSys RZIP model is a linear model that treats the plasma as a fixed spatial distribution of current, allowing for rigid radial and vertical motions.

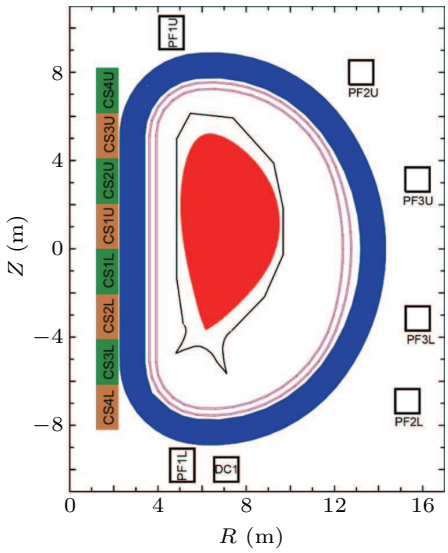


Fig. 1. CFETR standard LSN configuration.

Table 1. Main parameters of the CFETR.

Parameters	CFETR
Plasma current I_p (MA)	14
Toroidal field B_t (T)	6.5
Major radius R (m)	7.2
Minor radius a (m)	2.2
Elongation k	2.0
Plasma shape	LSN

Table 2. Geometric parameters of the CFETR poloidal field coils.

Coils	R (m)	Z (m)	dR	dZ	Turns
CS1U	1.70	1.025	1.0	2.05	738
CS2U	1.70	3.075	1.0	2.05	738
CS3U	1.70	5.125	1.0	2.05	738
CS4U	1.70	7.175	1.0	2.05	738
CS4L	1.70	–5.125	1.0	2.05	738
CS3L	1.70	–3.075	1.0	2.05	738
CS2L	1.70	–1.025	1.0	2.05	738
CS1L	1.70	–4.995	1.0	2.05	738
PF1U	4.60	9.80	1.1	1.5	448
PF2U	13.20	8.00	1.1	1.1	225
PF3U	15.73	3.15	1.1	1.1	225
PF1L	4.60	–9.80	1.1	1.5	448
PF2L	15.30	–6.90	1.1	1.1	225
PF3L	15.73	–3.15	1.1	1.1	225
DC1	7.10	–10.00	1.1	1.1	225

The remainder of this paper is organized as follows. Section 2 briefly introduces the modelling of CFETR in TSC. The free-drift analysis of CFETR and calculation of the vertical instability growth rate of CFETR are presented in Sections 3 and 4, respectively. Section 5 describes the robust control analysis and performance assessment by scanning typical IC locations of CFETR, validated by TokSys. Finally, Section 6 provides a summary of the study.

2. Two-dimensional modelling of CFETR in TSC

Each coil pack has a width of dR and a height of dZ, with its center located at coordinates (R, Z). Within the winding packs, the number of columns and rows is denoted as NR and NZ, respectively. The superconducting coil system of CFETR comprises eight central solenoid (CS) coils, six poloidal field (PF) coils, and one additional divertor-configuration coil (DC1). The main components associated with vertical displacement control are 16 toroidal field (TF) coils, a double-layer vacuum chamber, and a blanket structure. The actual engineering design of the blanket structure mainly includes the first wall (FW), tritium propagation zone, back plate + manifold, and back support structure (BSS). Its complex engineering structure cannot be directly used to evaluate the controllability of vertical displacement, so it is necessary to conduct physical modelling of it. Focusing on the blanket structure designed by CFETR, two-dimensional models of the blanket structure, vacuum chamber, and PF coils were simplified and constructed based on the engineering design structure of CFETR, as shown in Fig. 2. Using these models,[12] a device mechanism model of CFETR was implemented in TSC, as depicted in Fig. 3.

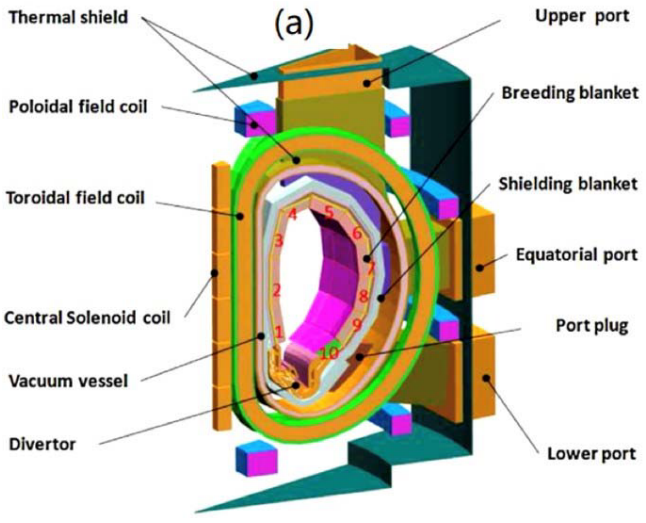


Fig. 2. Blanket and vacuum chamber engineering design.

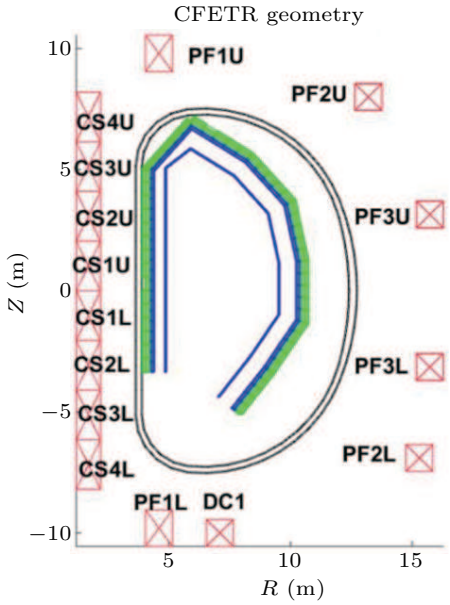


Fig. 3. Physical modelling of CFETR VDE based on engineering design.

3. CFETR free drift discharge simulation

In order to simulate a VDE process, the initial plasma equilibrium of CFETR needed to be constructed according to the listed coil currents and key plasma equilibrium parameters, such as plasma current I_p, major radius R_0, plasma vertical position Z_c, elongation κ, poloidal beta β_P, and internal inductance l_i. Table 3 lists the coil currents for the initial equilibrium establishment of CFETR by TSC, compared with the EFIT simulation results.[13] As shown in Fig. 4, the TSC reconstructed equilibrium (black) was consistent with the standard target (red) shape of the EFIT.[14,15] It provides a foundation for CFETR free-drift simulation, growth rate calculation, and vertical displacement instability control.[16–18]

Table 3. Initial equilibrium coil current of CFETR.

PF	Group	TSC (kA/turn)	EFIT (kA/turn)
CS1U	1	−4.505	−4.505
CS2U	2	0.399	0.399
CS3U	3	6.014	6.014
CS4U	4	7.239	7.239
CS4L	5	23.929	23.929
CS3L	6	25.874	25.874
CS2L	7	−5.202	−5.202
CS1L	8	−14.360	−14.360
PF1U	9	29.971	29.971
PF2U	10	8.889	8.889
PF3U	11	−34.730	−32.730
PF1L	12	38.918	38.918
PF2L	13	−37.220	−37.220
PF3L	14	−5.337	−4.337
DC1	15	8.153	8.153

The design of the feedback control system depends on the calculation of the plasma instability growth rate and the reasonable reliability of the control model. Based on the initial plasma equilibrium above, all feedback control systems were turned off, and TSC completed the predictive simulation of the CFETR free-drift process.[19–24] As presented in Fig. 5, with the feedback system off, the plasma vertical position became uncontrollable and drifted upward. Meanwhile, with the plasma position out of control, the plasma current also attenuated, as shown in Fig. 6. Without effective control, this will lead to a vertical displacement instability event, plasma disruption, and discharge termination.

I_p (MA)	R_m (m)	Z_m (m)	Kappa	β_p	Li (3)
13	7.539	0.766	1.99	1.16	0.74

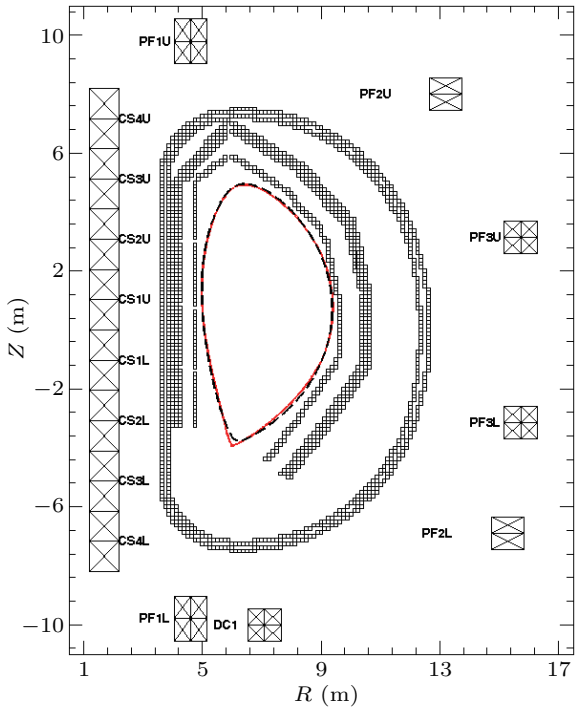


Fig. 4. Establishment of CFETR initial equilibrium.

4. Calculation of CFETR vertical instability growth rate

For tokamaks with non-circular cross sections, plasma vertical instability exists because the attenuation exponent of the vertical field is negative. If not properly controlled, it is prone to triggering a vertical displacement event. The plasma will move upward or downward within a few milliseconds and eventually touch the first wall of the vacuum chamber, leading to its disruption. This will pose a great threat to the safety of the first wall, vacuum chamber, and ohmic heating coil, so the vertical displacement event must be suppressed. The control of VDE depends on the magnitude of its growth rate, making the calculation of the growth rate particularly critical. By directly solving the motion equation of the plasma, the resistive MHD equations can accurately simulate the interaction between the plasma and the surrounding conductors such as passive feedback plates and active feedback coils. We simulate a typical disruption process of CFETR due to the occurrence of a vertical displacement event. When calculating the growth

rate of VDE, the vertical position of the plasma is expressed as

$$z(t) = z_0 + \delta z(t), \tag{1}$$

where z_0 is the plasma position at equilibrium at the initial moment. Suppose a VDE takes place at time t_0. The plasma is considered to have a small vertical displacement $\delta Z(t_0)$ at the initial time. The evolution of vertical displacement with time can be expressed as[25,26]

$$Z(t) = Z_0 + \delta Z(t) \approx Z_0 + \delta Z(t_0)\,\mathrm{e}^{\lambda(t-t_0)}. \tag{2}$$

When feedback control of the vertical position is deactivated, the instability eigenvalue of the closed-loop system is equal to that of the open-loop linear tokamak model, denoted by λ. λ is also referred to as the growth rate, γ. Under this condition, from the initial VDE onset time t_0 to any arbitrary time t, $\lambda(t-t_0)$ is the time integral of the instability growth rate γ. The expression is as follows:

$$\lambda(t-t_0) = \int_{t_0}^{t} \gamma \,\mathrm{d}\tau. \tag{3}$$

Equation (2) is changed to

$$Z(t) = Z_0 + \delta Z(t_0)\,\mathrm{e}^{\int_{t_0}^{t}\gamma(\tau)\,\mathrm{d}\tau}. \tag{4}$$

It is actually a solution to the first-order differential equation of Eq. (5)

$$\frac{\mathrm{d}Z}{\mathrm{d}t} = \gamma(t)\delta Z(t_0)\,\mathrm{e}^{\int_{t_0}^{t}\gamma(\tau)\,\mathrm{d}\tau} = \gamma(t)(Z - Z_0). \tag{5}$$

The hypothesis is that z_0 and $\delta z(t_0)$ are constant values, the growth rate γ is a function of time t, and t_0 is the beginning of the VDE.

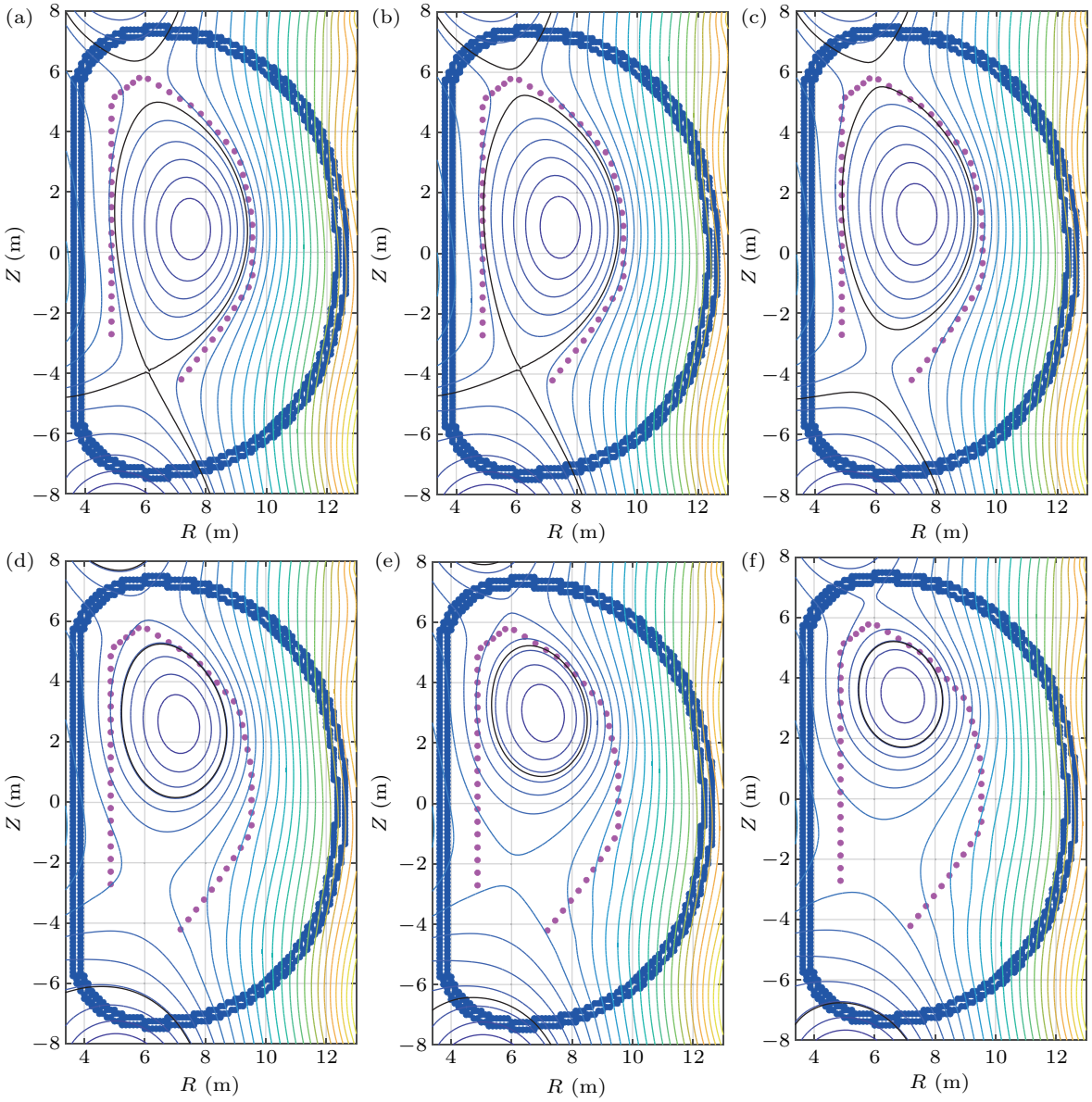


Fig. 5. The plasma configuration evolution of CFETR free drift.

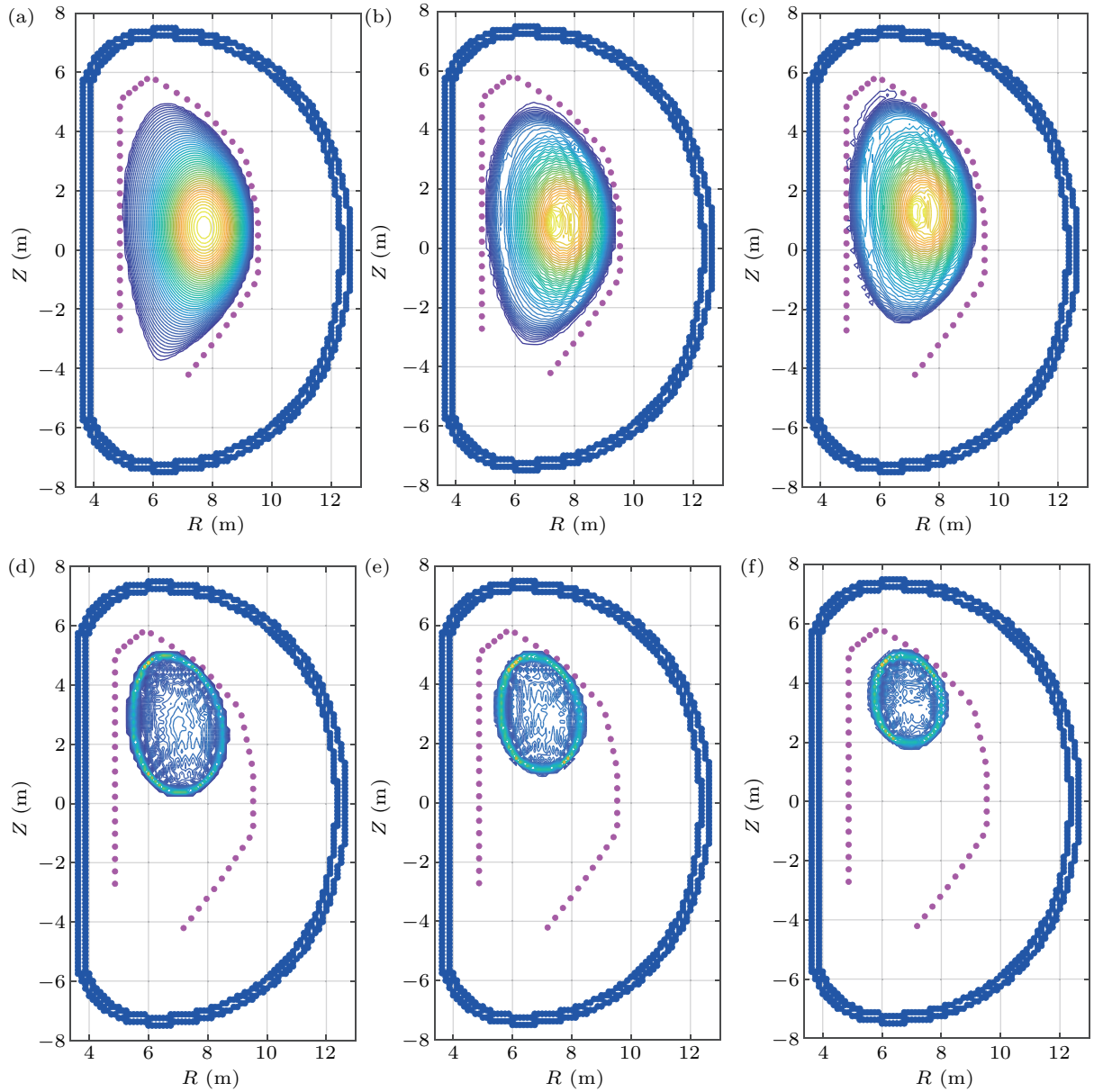


Fig. 6. The plasma current profile evolution during CFETR free drift.

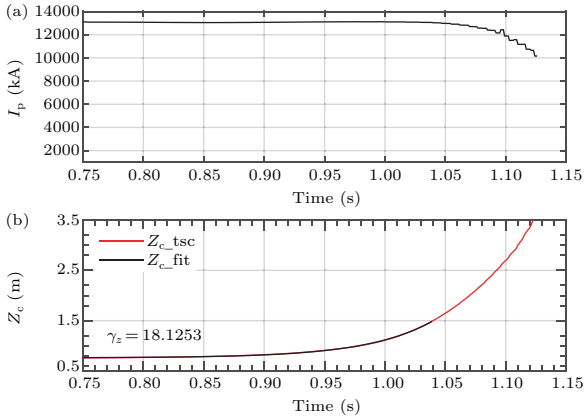


Fig. 7. TSC simulation of CFETR free drift.

From Eq. (4), the actual displacement away from the equilibrium position after VDE is obtained:

$$\tilde{Z} = Z(t) - Z_0 = \delta Z(t_0)\, \mathrm{e}^{\int_{t_0}^{t} \gamma(\tau)\,\mathrm{d}\tau}, \tag{6}$$

$$\ln|\tilde{Z}| = \ln|\delta Z(t_0)| + \int_{t_0}^{t} \gamma(\tau)\,\mathrm{d}\tau. \tag{7}$$

Finally, the growth rate is obtained as

$$\frac{\mathrm{d}\ln|\tilde{Z}|}{\mathrm{d}t} = \gamma(t). \tag{8}$$

Figure 7 shows the temporal evolution of the plasma magnetic axis. The red line represents the TSC simulation results, and the black line represents the fitted data. The TSC simulation results are in excellent agreement with the fitted data. Based on this, the plasma magnetic axis coordinate Z_c in Fig. 7 was substituted into Eqs. (6) and (8) to calculate the growth rate of the plasma vertical displacement event (VDE). The results indicate that the vertical instability growth rate for CFETR is $\gamma = 18.1253\ \mathrm{s}^{-1}$, which is close to the TokSys result ($\gamma = 18.1\ \mathrm{s}^{-1}$), as illustrated in Fig. 7. It demonstrates that the

passive structure (vacuum chamber + blanket) can only delay, but cannot provide sufficient passive stabilization, and must be actively controlled by the internal coil IC.

5. CFETR vertical displacement instability active control model and IC position optimization

5.1. CFETR vertical displacement instability control model

The feedback modes of vertical displacement events (VDEs) can be divided into passive feedback and active feedback. Once the plasma undergoes vertical displacement, eddy currents are immediately induced in the surrounding conductors (such as the vacuum chamber wall conductor), which hinder the vertical drift of the plasma. However, due to the resistance of the conductor, the eddy currents dissipate. When the time scale exceeds the diffusion time of the conductor τ_R, the passive effect can no longer maintain the vertical position of the plasma. Therefore, active feedback must be employed for slow disturbances with a time scale larger than τ_R. The classical proportional-derivative (PD) control model is adopted in this study. Active feedback collects the plasma vertical displacement signal and feeds it back to the main control power system in a certain way, thereby supplying current to the active feedback coils to achieve the purpose of controlling the plasma. In the vacuum chamber, IC1 and IC2 are a pair of plane-symmetric active feedback coils in the relative device. Equivalent reverse currents are passed through them to generate a magnetic field along the horizontal direction, so as to achieve feedback control of the plasma in the vertical direction[27]

$$I_f = g_p(Z_{mag} - Z_0) + g_d \frac{d}{dt}(Z_{mag} - Z_0), \tag{9}$$

where Z_{mag} represents the vertical position of the collected plasma magnetic axis, Z_0 represents the expected position of the plasma magnetic axis, and g_p and g_d are proportional and differential factors, respectively. Here, the vertical position Z_{mag} of the plasma magnetic axis can be measured for feedback control. When the measured Z_{mag} deviates from the expected value Z_0, the control system will initiate feedback control and calculate the feedback current required to pull the plasma with vertical displacement back to the original equilibrium position Z_0.

5.2. Optimization of IC position of CFETR fast control coil

The computational grid is defined over the range 3.375 m$< R <$ 13.00 m, $-$8.00 m$< Z <$ 8.00 m, with a grid resolution of 78 $\times$ 129 points and a mesh size of 0.125 m $\times$ 0.125 m. According to the three-dimensional structure of the CFETR coils, vacuum chamber, and blanket, the equivalent two-dimensional model of CFETR is constructed, as shown in Fig. 4.

The IC coil parameter selection range is $R \sim$ 11.975–12.025 m, dr = 0.20 m, dz = 0.20 m. In the design of the internal coil layout, there were three options for CFETR VS coil fixation, consistent with TokSys: the vacuum interior wall, the outer wall of the blanket, and the inner wall of the blanket. The specific locations of these coils (shown in Fig. 8) are as follows: Location 1 (11.5, 3.3) m, (11.5, $-$3.3) m, with 6 turns; Location 2 (10.5, 4.4) m, (9.5, $-$3.6) m, with 6 turns; Location 3 (8.95, 4.4) m, (7.9, $-$4.4) m, with 6 turns.

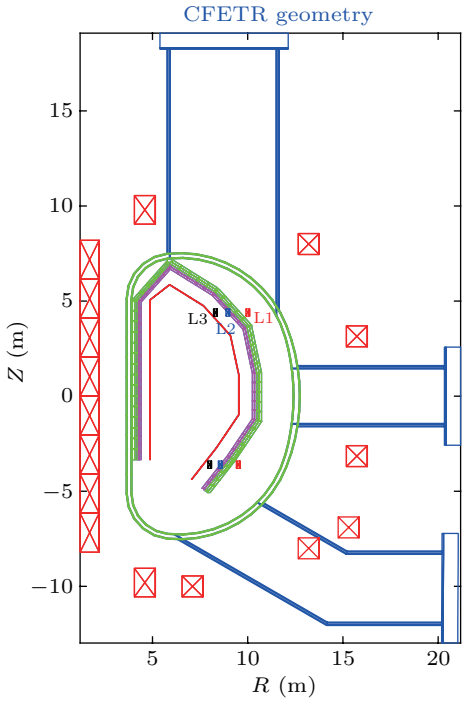


Fig. 8. TSC modelling and IC using three typical locations.

5.3. Design of control current waveforms for CFETR vertical displacement instability

The three typical locations of the IC coils shown in Fig. 8 are as follows: Location 1: IC1 (11.5 m, 3.3 m), IC2 (11.5 m, $-$3.3 m), mounted on the inner vacuum vessel wall, with 6 turns each (Fig. 9); Location 2: IC1 (10.5 m, 4.4 m), IC2 (9.5 m, $-$3.6 m), mounted on the outer wall of the blanket, with 6 turns each (Fig. 10); Location 3: IC1 (8.95 m, 4.4 m), IC2 (7.9 m, $-$4.4 m), mounted on the inner wall of the blanket, with 6 turns each (Fig. 11). In order to avoid the loss of control of vertical position (safe control), the maximum controllable displacement should be no less than 5%·a, and 10%·a should be achieved for robust control, where a denotes the tokamak minor radius. Therefore, for the three typical IC coil locations mentioned above, under the conditions of Δz_{max} = 22 cm and $\Delta z_{max}/a$ = 10%, the IC coil current waveforms under robust control mode are shown below.[28,29]

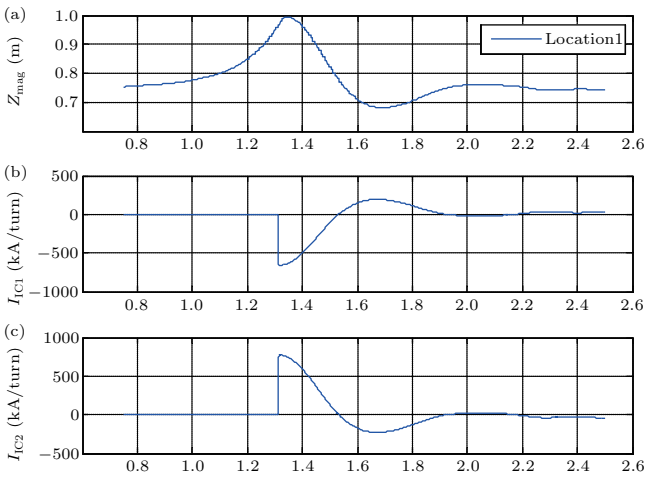


Fig. 9. IC current waveform at Location 1 under robust control mode.

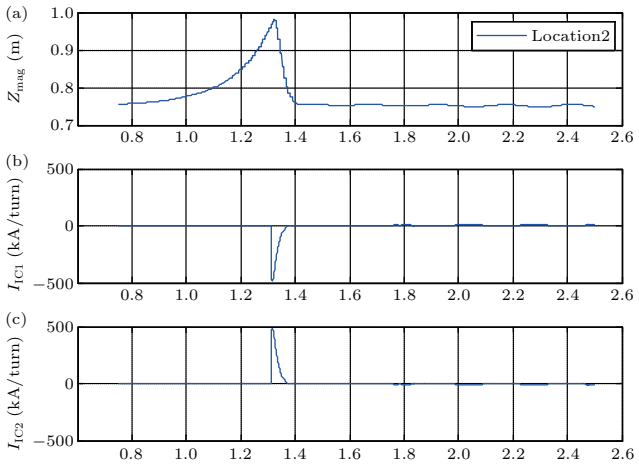


Fig. 10. Current waveform of IC in Location 2 under robust control mode.

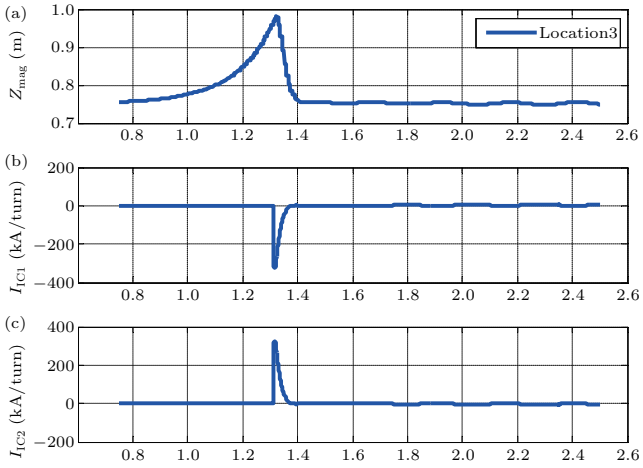


Fig. 11. Current waveform of IC in Location 3 under robust control mode.

Table 4. Robust control, TokSys/TSC simulation results comparison.

IC location	Multiple of blanket resistivity	Peak current of TokSys/kA·turns	Peak current of TSC/kA·turns
L1	5	674.8	674.8
L2	5	453.24	468
L3	5	316.8	320

By scanning IC coil locations shown in Fig. 8, the peak IC coil currents are determined as follows: 674.8 kA·turns at Location 1, 468 kA·turns at Location 2, and 320 kA·turns at Location 3. At the same time, Table 4 presents a comparison of the control effects of TokSys and TSC simulation results on the power supply capacity requirements when the "robust control" requirements are met (Z initial disturbance is 22 cm), 5 times the blanket resistivity is used, and the L1–L3 coil positions above are considered. The TSC results are consistent with the TokSys simulation results, indicating the reliability of the TSC results. Under the same displacement disturbance, the control effect of IC coils closer to the plasma is obviously better than that of those farther away, which can significantly reduce the demand for power supply capacity. Since Location 3 is located on the inner wall of the blanket and closer to the plasma, its interaction with the plasma is enhanced. In contrast, Location 1 and Location 2 are farther away from the plasma, which weakens their interaction with the plasma and reduces the plasma control performance. Meanwhile, the blanket exerts a certain shielding effect on Location 1 and Location 2, further lowering their control efficiency for plasma vertical instability. Thus, the results indicate that Location 3 is the most favorable.

In the above analysis of coil position optimization and power supply capacity requirements, engineering restrictions such as window limitations and neutron irradiation are not taken into account. The above designs represent the minimum power supply capacity requirements for the power supply system. Therefore, this work requires relevant engineering teams, including those responsible for device engineering design, power supply design, fast control coil design, and other related engineering groups, to conduct feasibility analysis and verification, ultimately achieving a balance between physical requirements and engineering realization capabilities.

Furthermore, besides the PD feedback model, alternative control strategies will be explored in the next phase of work. For example, trained neural networks and adaptive methods will be planned to examine the relationship between the vertical growth rate and key plasma parameters in the future.

6. Conclusion

In this study, the CFETR device was modeled using the TSC, generating a two-dimensional equivalent device geometry and an initial equilibrium configuration, as illustrated in Fig. 4. The plasma boundary computed by TSC (black) was verified against an EFIT reconstruction (red), showing good agreement.

The vertical growth rate γ is a key parameter for characterizing and controlling plasma vertical instability. Here, the free-drift plasma evolution in CFETR was simulated with

TSC, and the vertical growth rate during free drift was determined by fitting the trajectory of the vertical plasma position $Z_c(t)$, yielding $\gamma = 18.1253\ \mathrm{s}^{-1}$. This result is consistent with the value obtained from the TokSys code ($\gamma = 18.1\ \mathrm{s}^{-1}$) shown in Fig. 7, confirming the reliability of the simulation.

The efficiency of active vertical displacement control depends significantly on the positioning of the internal control (IC) coils shown in Fig. 8. To evaluate this dependence, robust feedback control of vertical displacement events (VDEs) was simulated in TSC for three representative IC configurations: Location 1 (IC coils positioned at (11.5 m, 3.3 m) and (11.5 m, −3.3 m) on the inner vacuum vessel wall), Location 2 (IC coils at (10.5 m, 4.4 m) and (9.5 m, −3.6 m) on the outer blanket wall), and Location 3 (IC coils at (8.95 m, 4.4 m) and (7.9 m, −4.4 m) on the inner blanket wall). For each configuration, the minimum power supply requirements for robust VDE control were analyzed and benchmarked against TokSys simulations shown in Table 4. The results indicate that Location 3 is the most favorable, requiring a peak current of 320 kA·turns for effective control. These findings offer important guidance for optimizing IC coil parameters to enhance stability margins and provide valuable input for the design of vertical stabilization systems in future tokamaks.

Acknowledgments

Project supported by the National Natural Science Foundation of China (Grant Nos. 12275307 and 12475210). Numerical simulations are carried out using the CFETR Integration Design Platform (CIDP) with the support of the Supercomputing Center of University of Science and Technology of China and the Shenma High Performance Computing Cluster (Institute of Plasma Physics, Chinese Academy of Sciences).

References

[1] Wesson J 1997 *Tokamaks* 2nd Edn. (New York: Oxford University Press) p. 318
[2] Sayer R O, Peng Y K, Jardin S C, Kellman A G and Wesley J C 1993 *Nucl. Fusion* **33** 969
[3] Song Y T, Wu S T, Li J G, Wan B N, Wan Y X, Fu P, Ye M Y, Zheng J X, Lu K, Gao X G, Liu S M, Liu X F, Lei M Z, Peng X B and Chen Y 2014 *IEEE Trans. Plasma Sci.* **42** 503
[4] Jardin S C, Bell M G and Pomphrey N 1993 *Nucl. Fusion* **33** 371
[5] Jardin S C, Pomphrey N and Delucia J L 1986 *J. Comput. Phys.* **66** 481
[6] Jardin S C, Kessel C E and Pomphrey N 1994 *Nucl. Fusion* **34** 1145
[7] Humphreys D A, Ferron J R, Bakhtiari M, Blair J A, In Y, Jackson G L, Jhang H, Johnson R D, Kim J S, Lahaye R J, Leuer J A, Penaflor B G, Schuster E, Walker M L, Wang H, Welander A S and Whyte D G 2007 *Nucl. Fusion* **47** 943
[8] Nakamura Y, Yoshino R, Neyatani Y, Tsunematsu T, Azumi M, Pomphrey N and Jardin S C 1996 *Nucl. Fusion* **36** 643
[9] Humphreys D A, Leuer J A and Walker M L 1999 *Proc. 41st Annu. Meet. Div. Plasma Phys.* p. 175
[10] Humphreys D A, Casper T A, Eidietis N, Ferrara M, Gates D A, Hutchinson I H, Jackson G L, Kolemen E, Leuer J A, Lister J, LoDestro L L, Meyer W H, Pearlstein L D, Portone A, Sartori F, Walker M L, Welander A S and Wolfe S M 2009 *Nucl. Fusion* **49** 115003
[11] Liu L, Xiao B J, Humphreys D A, Luo Z P and Chen S L 2014 *Fusion Eng. Des.* **89** 563
[12] Qiu Q L, Xiao B J, Guo Y, Liu L, Xing Z and Humphreys D A 2016 *Nucl. Fusion* **56** 106029
[13] Li H, Li G Q, Liu X J, Qian J P, Huang Y, Luo Z P, Guo Y, Liu X F, Liu L, Zheng J X, Liu S L, Gao X and CFETR Design Team 2020 *Fusion Eng. Des.* **152** 111447
[14] Lao L L, St. John H and Stambaugh R D 1985 *Nucl. Fusion* **25** 1611
[15] Yu Q Z, Huang Y, Luo Z P, Wang Y H, Liu Z J, Rui W Y, Wu K, Xiao B J and Li J G 2024 *Chin. Phys. B* **33** 045201
[16] Qian J P, Wan B N, Shen B, Walker M L, Humphreys D A and Xiao B J 2009 *Chin. Phys. B* **18** 2432
[17] Lackner K and Macmahon A B 1974 *Nucl. Fusion* **14** 575
[18] Jiang C Z, Wang S W, Zhou Z Y, Hu D, Li B and JOREK team 2024 *Chin. Phys. Lett.* **41** 085201
[19] Wu B and Zhang C 2003 *Plasma Sci. Technol.* **5** 1625
[20] Bandyopadhyay I, Ahmed S M, Atrey P K, Bhatt S B, Bhattacharya R, Chaudhury M B, Deshpande S P, Gupta C N, Jha R, Shankar J Y, Kumar V, Manchanda R, Raju D, Rao C V S, Vasu P and ADITYA Team 2004 *Plasma Phys. Control. Fusion* **46** 1443
[21] ITER Physics Basis Editors 1999 *Nucl. Fusion* **39** 2137
[22] Matsukawa M, Hosogane N and Ninomiya H 1992 *Plasma Phys. Control. Fusion* **34** 907
[23] Guo Y, Xiao B J, Liu L, Yang F, Wang Y H and Qiu Q L 2016 *Chin. Phys. B* **25** 115201
[24] Kessel C E, Heitzenroeder P and Jun C 2001 *Nucl. Fusion* **41** 953
[25] Qiu Q L, Xiao B J, Guo Y, Liu L and Wang Y H 2017 *Chin. Phys. B* **26** 065205
[26] Liu L 2008 *Simulation of Vertical Instability and Feedback Control in EAST* (Master Dissertation) (Hefei: Institute of Plasma Physics, Chinese Academy of Sciences) (in Chinese)
[27] Kessel C E, Giruzzi G, Sips A C C, Budny R V, Artaud J F, Basiuk V, Imbeaux F, Joffrin E, Schneider M, Murakami M, Luce T, Holger S J, Oikawa T, Hayashi N, Takizuka T, Ozeki T, Na Y S, Park J M, Garcia J and Tucillo A A 2007 *Nucl. Fusion* **47** 1274
[28] Kessel C E, Mau T K, Jardin S C and Najmabadi F 2006 *Fusion Eng. Des.* **80** 63
[29] De Tommasi G, De Grazia L E, Dubbioso S, Fiorenza F, Frattolillo D, Inoue S, Mattei M, Pironti A and Urano H 2024 *Nucl. Fusion* **64** 076005